

Revealing topological superconductivity in extended quantum spin Hall Josephson junctions

Shu-Ping Lee,¹ Karen Michaeli,² Jason Alicea,¹ and Amir Yacoby³

¹*Department of Physics and Institute for Quantum Information and Matter,
California Institute of Technology, Pasadena, CA 91125, USA*

²*Department of Condensed Matter Physics, Weizmann Institute of Science, Rehovot, 76100, Israel*

³*Department of Physics, Harvard University, Cambridge, Massachusetts 02138 USA*

Quantum spin Hall-superconductor hybrids are promising sources of topological superconductivity and Majorana modes, particularly given recent progress on HgTe and InAs/GaSb. We propose a new method of revealing topological superconductivity in extended quantum spin Hall Josephson junctions supporting ‘fractional Josephson currents’. Specifically, we show that as one threads magnetic flux between the superconductors, the critical current traces an interference pattern featuring sharp fingerprints of topological superconductivity—even when noise spoils parity conservation.

Introduction. ‘Spinless’ one-dimensional (1D) topological superconductors [1–5] host various novel phenomena, most notably Majorana zero-modes that lead to non-Abelian statistics and, in turn, fault-tolerant quantum information applications [6]. Among numerous plausible realizations [7–12], Fu and Kane’s early proposal for nucleating 1D topological superconductivity at a quantum spin Hall (QSH)/superconductor interface remains a leading contender. Inducing a superconducting proximity effect in the QSH system indeed very naturally produces topological superconductivity—neither careful tuning of the Fermi level nor time-reversal symmetry breaking are required, the latter feature underpinning intrinsic resilience to disorder [13]. Experiments have, moreover, shown exciting recent progress, with QSH behavior *and* good proximity effects conclusively demonstrated in both HgTe [14–18] and InAs/GaSb [19–22] quantum wells.

In light of these developments, the following question becomes paramount: How can one compellingly reveal topological superconductivity in these QSH setups? Most detection protocols to date focus on tunneling [23–25] and Josephson [7, 26–36] anomalies. The latter originate from the ‘fractional Josephson effect’ [1] wherein a phase twist $\delta\phi$ across a topological superconductor yields a supercurrent with 4π periodicity in $\delta\phi$ —twice that of conventional junctions. One can view the doubled periodicity as arising from a pair of hybridized Majorana modes at the junction, which form an unusual Andreev bound state that mediates supercurrent via single electron (rather than Cooper pair) tunneling. In the simplest case this anomalous current takes the form $I_{4\pi} \propto (-1)^p \sin(\delta\phi/2)$, where the parity $p = 0, 1$ denotes the Andreev bound state’s occupation number. Directly observing this spectacular effect is, however, nontrivial. Parity switching processes—which send $p \rightarrow 1 - p$ and can arise, *e.g.*, from quasiparticle poisoning—restore 2π periodicity to the current unless measurements occur on a time scale short compared to the typical parity-flip time. (Long-time-scale measurements may still reveal subtler signatures of topological superconductivity [27, 31, 32, 36], for instance through noise.)

Inspired by recent experiments by Hart *et al.* [18], we study transport in an extended Josephson junction bridged by a QSH insulator; see Fig. 1. This setup is expected to host two 1D topological superconductors that produce ‘parallel’ fractional

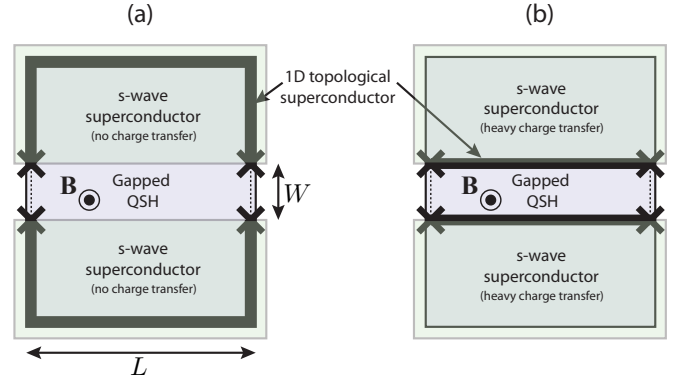


FIG. 1. (color online). Extended QSH Josephson junctions that host 1D topological superconductivity. Topological superconductors reside either (a) at the outer boundary or (b) across the barrier depending on whether the superconductors dope the contacted QSH regions.

Josephson currents at the junction ends. One virtue of such extended junctions is that the critical current $I_c(\Phi)$, measured as a function of magnetic flux Φ passing between the superconductors, displays an interference pattern that can reveal detailed information about the nature of current flow. For example, in HgTe junctions similar to those examined here Hart *et al.* observed an interference pattern indicating current sharply peaked at the edges [18], precisely as expected with a QSH-insulator barrier. Here we ask whether such interference measurements can also provide fingerprints of 1D topological superconductivity—which again ought to naturally form in this setting.

Our central result is that the fractional Josephson effect indeed imprints qualitative signatures of topological superconductivity on the junction’s interference pattern and the corresponding critical current, *even when parity switching processes are abundant*. If parity relaxes to minimize the energy, the critical current remains finite at any magnetic flux contrary to conventional symmetric junctions. Still more striking signatures appear if parity instead flips randomly on suitably long time scales—multiple critical currents are visible in the current-voltage traces, and the lower critical current *vanishes* at zero flux provided the fractional Josephson currents

dominate. These results highlight relatively simple dc measurements that can reveal 1D topological superconductivity in QSH junctions and related platforms.

Extended Josephson junction model. Following Ref. [18] we consider two *s*-wave superconductors deposited on a QSH material to create an extended Josephson junction of barrier width W and length L (see Fig. 1). Suppose first that the QSH system's chemical potential resides everywhere in the bulk gap, and that the superconductors merely induce pairing via the proximity effect. The edge states along the perimeter then form 1D topological superconductors [7] that hybridize at the junction as Fig. 1(a) illustrates. Due to work-function mismatch, however, we expect that in practice the superconductors additionally transfer charge and shift the local Fermi level in the contacted QSH regions well into the bulk bands (though the barrier can still remain depleted). To address this more realistic scenario, note that one can always change the sign of the mass for the heavily doped regions without closing a gap. The outer regions then admit a trivial band structure—hence edge states occur *only* at the boundary of the smaller QSH insulator comprising the barrier. As shown in Fig. 1(b) these edge modes form 1D topological superconductors due to proximity with the adjacent superconductors; their hybridization yields the same physics as in Fig. 1(a). The ‘migration’ of topological superconductivity described here is reminiscent of Ref. [37] and could be useful, *e.g.*, for synthesizing networks for braiding [3, 23].

For simplicity we assume negligible edge-state penetration depth and $W \ll \xi$ and $L \gg \xi$ throughout, with ξ the coherence length of the 1D topological superconductors. In this limit the left/right junction ends each support a single Andreev bound state with energy $(-1)^{p_{L/R}} \Delta \cos(\delta\phi_{L/R}/2)$. Here Δ is the induced pairing energy while $p_{L/R}$ and $\delta\phi_{L/R}$ respectively denote the parity and phase difference at the left/right sides. Generally, $\delta\phi_{L/R}$ follow from the phase difference ϕ between the two superconductors and the number of flux quanta $f = \Phi/(h/2e)$ threading the barrier—*i.e.*, $\delta\phi_L = \phi$ and $\delta\phi_R = \phi + 2\pi f$. Defining a vector $\mathbf{p} = (p_L, p_R)$, the bound states together contribute an energy

$$E_{\mathbf{p}}(\phi, f) = \Delta[(-1)^{p_L} \cos(\phi/2) + (-1)^{p_R} \cos(\phi/2 + \pi f)] \quad (1)$$

and a Josephson current $I_{\mathbf{p}}(\phi, f) = \frac{e}{\hbar} \partial_{\phi} E_{\mathbf{p}}(\phi, f)$.

We consider a current-biased junction and extract the $I - V$ characteristics using an over-damped RCSJ model [38]. The total injected current I derives from two parallel channels: the Josephson current and resistive sources such as normal quasiparticles characterized by a resistance R . The former—which we temporarily assume consists only of $I_{\mathbf{p}}$ —shunts the resistive component $I_N = V/R = \hbar\dot{\phi}/(2eR)$ provided the junction does not generate voltage. *Between two parity-switching events* the phase ϕ thus evolves according to

$$I = I_{\mathbf{p}}(\phi, f) + \frac{\hbar}{2eR} \dot{\phi} + \zeta(t), \quad (2)$$

where the last term reflects a thermal noise current satisfying

$\langle \zeta(t)\zeta(t') \rangle = 2T/R\delta(t - t')$ (T denotes the junction temperature; throughout we assume $T \ll \Delta$). Equation (2) describes a strongly damped particle with coordinate ϕ in a ‘tilted washboard’ potential $U_{\mathbf{p}}(\phi, f) = E_{\mathbf{p}}(\phi, f) - \hbar I \phi/e$. For sufficiently small I the potential favors pinning the particle to one of its minima. Random thermal noise allows the particle to escape over the barrier [39], whereupon the frictional force $\hbar\dot{\phi}/2eR$ causes relaxation to a new minimum on a time scale proportional to $\tau_R \equiv \hbar^2/(4e^2 R \Delta)$. No minima exist above a parity-dependent critical current; the particle then rolls unimpeded down the potential, generating a substantial voltage.

Parity-switching events transfer the particle between different tilted washboard potentials ($U_{\mathbf{p}} \rightarrow U_{\mathbf{p}'}$) and thus provide an additional route for the phase ϕ to diffuse even at zero temperature. Our goal now is to quantify the effects of parity switching on transport in various interesting regimes.

Fokker-Planck analysis. To this end let $\mathcal{P}_{\mathbf{p}}(\phi, t)$ be the distribution function that describes the probability of finding the system with parities \mathbf{p} and phase ϕ at time t . This function obeys a generalized Fokker-Planck equation:

$$\partial_t \mathcal{P}_{\mathbf{p}} = \frac{1}{\tau_R \Delta} \partial_{\phi} [\partial_{\phi} U_{\mathbf{p}}/2 + T \partial_{\phi}] \mathcal{P}_{\mathbf{p}} + \sum_{\mathbf{p}'} [W_{\mathbf{p}' \rightarrow \mathbf{p}} \mathcal{P}_{\mathbf{p}'} - W_{\mathbf{p} \rightarrow \mathbf{p}'} \mathcal{P}_{\mathbf{p}}], \quad (3)$$

where the first line describes thermal phase diffusion along the tilted washboard potential $U_{\mathbf{p}}$ with fixed parity [39, 40] while the second incorporates parity switching with rates $W_{\mathbf{p} \rightarrow \mathbf{p}'}$. Equation (3) implicitly assumes that parity-flip processes do not involve an instantaneous change in the phase ϕ ; this holds provided the time scale for such events is the shortest in the problem. We further postulate a phenomenological parity-switching mechanism whereby a particle bath connected to the Josephson junction allows electrons to hop into and out of the bound states. We model the corresponding transition rate from parity configuration \mathbf{p} to \mathbf{p}' by

$$W_{\mathbf{p} \rightarrow \mathbf{p}'}(\phi, f) = \frac{n[(U_{\mathbf{p}'}(\phi, f) - U_{\mathbf{p}}(\phi, f))/T_b]}{\tau} \times [\delta_{p_R, p'_R} \delta_{p_L, 1-p'_L} + \delta_{p_R, 1-p'_R} \delta_{p_L, p'_L}], \quad (4)$$

with $1/\tau$ the typical parity-switching rate, $n[x] = (e^x + 1)^{-1}$ the Fermi distribution function, and T_b the bath temperature (which can differ from the junction temperature T). We only consider independent parity flips at the two junction sides—hence the Kronecker delta's in Eq. (4). The Supplementary Material further motivates these transition rates.

The junction's *dc* voltage V is determined by stationary solutions of Eq. (3). More precisely, the Josephson relation along with Eq. (2) yield

$$V = \frac{\hbar}{2e} \langle \dot{\phi} \rangle = \frac{\hbar}{2e} \sum_{\mathbf{p}} \int_0^{4\pi} d\phi \dot{\phi} \mathcal{P}_{\mathbf{p}}(\phi) = R \sum_{\mathbf{p}} \int_0^{4\pi} d\phi [I - I_{\mathbf{p}}(\phi, f)] \mathcal{P}_{\mathbf{p}}(\phi). \quad (5)$$

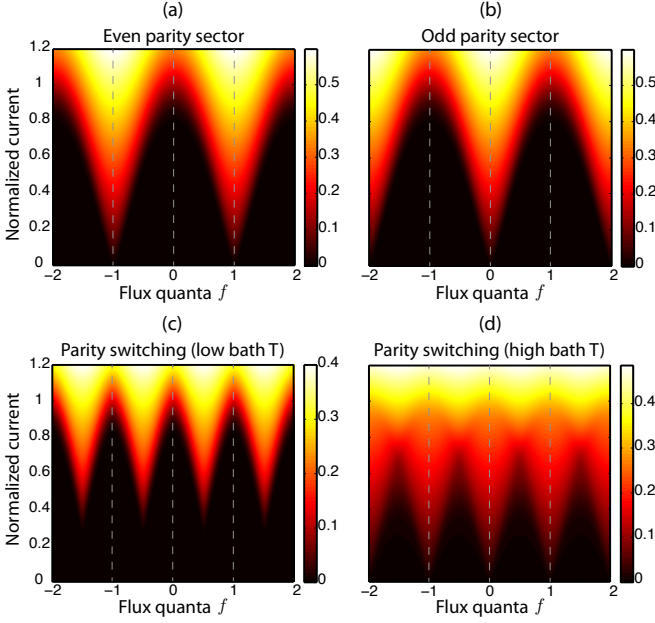


FIG. 2. (color online). Interference patterns in (a,b) the parity-conserving limit and (c,d) with parity switching at low ($T_b = 0.02\Delta$) and high ($T_b = 100\Delta$) bath temperature. Anomalies indicative of topological superconductivity arise in all cases. The color scale indicates voltage in units of $2eR\Delta/\hbar$ while current is normalized by $e\Delta/\hbar$. Data correspond to (a,b) $T = 0.05\Delta$, $\tau = 50\tau_R$, and (d) $T = 0.02\Delta$, $\tau = 5\tau_R$.

Determining the $I - V$ characteristics thus reduces to solving Eq. (3) for the steady-state distribution function $\mathcal{P}_{\mathbf{p}}(\phi)$, which is readily achieved numerically by discretizing ϕ . Below we briefly discuss the solution with conserved parity ($1/\tau = 0$) and then address the more realistic case where parity switching occurs.

When the parities \mathbf{p} are conserved the generalized Fokker-Planck equation admits four steady-state solutions—one for each parity sector. The solutions coincide with the known Ambegaokar-Halperin expressions [39] evaluated with an unconventional current-phase relation $I_{\mathbf{p}}(\phi, f)$. At $T = 0$ the voltage follows as [38, 39]

$$V = \Theta(I - I_{\mathbf{p},c})R\sqrt{I^2 - I_{\mathbf{p},c}^2}, \quad (6)$$

where $\Theta(x)$ is the Heaviside step function and the critical currents are $I_{\mathbf{p},c} = e\Delta|\cos(\pi f/2)|/\hbar$ for $p_R = p_L$ and $I_{\mathbf{p},c} = e\Delta|\sin(\pi f/2)|/\hbar$ for $p_R \neq p_L$. Thermally induced 4π phase slips at fixed \mathbf{p} produce a finite voltage at $T > 0$ even for $I < I_{\mathbf{p},c}$. Figures 2(a) and (b) respectively illustrate the low-temperature interference patterns in the even- and odd-parity sectors (the color scale represents the voltage V). Both cases exhibit an anomalous two-flux-quanta periodicity—a striking yet fragile fingerprint of topological superconductivity. Any finite switching rate $1/\tau \neq 0$ spoils this property, though as we now describe other signatures of topological superconductivity nevertheless persist.

For $1/\tau \neq 0$ Eq. (3) admits only one stationary solution

due to parity flip processes. Consider first low bath temperatures ($T_b \ll \Delta$) where the transition rates in Eq. (4) depend strongly on the relative energies in different parity sectors. The behavior then resembles that of a thermalized junction: to a good approximation parities switch only at energy crossings and adjust so that the system follows a washboard potential $U(\phi, f) = \min_{\mathbf{p}} U_{\mathbf{p}}(\phi, f)$ corresponding to a minimum energy. The $T \rightarrow 0$ and $T_b \rightarrow 0$ critical current—*i.e.*, the maximal I for which $\partial_{\phi} U_{\mathbf{p}}(\phi, f) = 0$ admits a solution—follows as $I_c = e\Delta/\hbar \max\{\cos^2(\pi f/2), \sin^2(\pi f/2)\}$. Figure 2(c) displays the numerically computed interference pattern at small but finite T and T_b (which includes thermal phase slips that smear the critical current, as in conventional junctions). The critical current clearly remains finite for all fluxes and, roughly, follows the larger of the critical currents present in the parity-conserving cases shown in Figs. 2(a) and (b). Here the absence of nodes is a remnant of the unconventional current-phase relation rooted in topological superconductivity. Other node-lifting sources also of course exist but can be distinguished from this mechanism as discussed below.

Finally, we analyze the most interesting limit—high bath temperature ($T_b \gg \Delta$), where the parities fluctuate randomly, independent of the initial and final energies, on a time scale τ . Here there are three distinct current regimes separated by the critical currents $I_{c1} = \min_{\mathbf{p}} I_{\mathbf{p},c}$ and $I_{c2} = \max_{\mathbf{p}} I_{\mathbf{p},c}$. For $I < I_{c1}$ local minima exist in the washboard potentials $U_{\mathbf{p}}$ for all four parity sectors. Nevertheless, even at $T = 0$ —where thermal diffusion is absent—the phase ϕ can still transform between minima of $U_{\mathbf{p}}$ via parity-switching events; see Figs. 3(a) and (b). The voltage resulting from such processes depends on the ratio of τ to the typical time τ_{rel} required for ϕ to relax to a washboard-potential minimum following a parity flip:

$$\tau_{\text{rel}} \sim \max_{\mathbf{p}} \frac{\hbar}{eR\sqrt{I_{\mathbf{p},c}^2 - I^2}}. \quad (7)$$

(A similar time scale emerges in the *ac* fractional Josephson effect [36].)

For $\tau \gg \tau_{\text{rel}}$ the phase ϕ has sufficient time to reach the nearest minimum of the new potential before parity switches again. After two consecutive parity flips ϕ either returns to its initial value or, as Figs. 3(a) and (b) illustrate, shifts by $\pm 2\pi$. The 2π and -2π phase changes occur with essentially equal probability when $T_b \gg \Delta$, and moreover contribute equal but opposite voltages. Hence these processes cancel one another in the *dc* limit. In other words, parity switching events generate telegraph noise in the voltage with equal probability of positive and negative signals that time-average to zero. As the current approaches I_{c1} , the relaxation time τ_{rel} grows and eventually exceeds the parity-flip time τ . Consecutive switching events then occur before the phase relaxes to the potential minima; the result is a net diffusion of ϕ down the washboard potentials, producing a finite voltage. This argument implies that in the limit $\tau \ll \hbar/(eRI_{c1})$ any current generates a non-zero voltage—*i.e.*, the critical current vanishes.

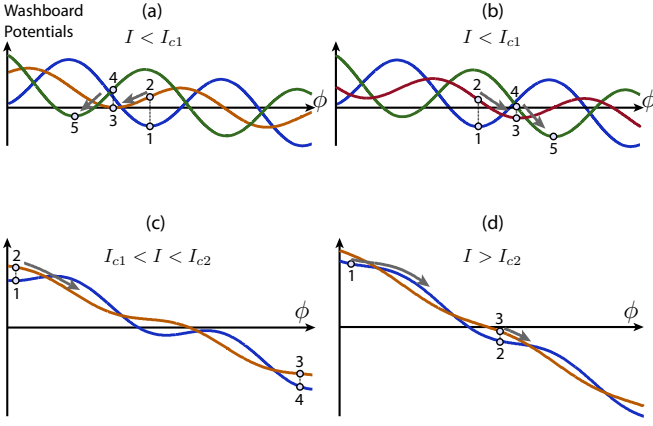


FIG. 3. (color online). Washboard potentials for different parity sectors (not all are shown) in the three high-bath-temperature current regimes. Numbers indicate sequential phase evolution steps. For low currents $I < I_{c1}$ all potentials exhibit minima, though consecutive parity flips can still mediate $\pm 2\pi$ phase slips as in (a) and (b). The voltage from these processes averages to zero if the parity relaxation time τ is sufficiently long. In (c) and (d) a finite voltage always develops; when $I_{c1} < I < I_{c2}$ the signal is reduced since half of the potentials exhibit minima that partially trap the phase.

With currents between I_{c1} and I_{c2} only two of the washboard potentials exhibit stable minima. Because of the high bath temperature, the phase ϕ can escape from one of these minima via a parity-switching event into a potential without any minima, producing a steady drift of ϕ . The drift ceases only when a subsequent parity flip re-traps the phase; see Fig. 3(c) for an illustration. Assuming $\tau \gg \tau_{\text{rel}}$, the phase drift generates a finite *dc* voltage $V \approx \mathcal{F}_{\text{drift}} R \sqrt{I^2 - I_{c1}^2}$ with $\mathcal{F}_{\text{drift}}$ the fraction of time spent in potentials without minima ($\mathcal{F}_{\text{drift}} \approx 1/2$ when $T_b \gg \Delta$). For currents close to I_{c2} the phase relaxation time τ_{rel} exceeds τ ; the phase can then essentially never reach a minimum due to frequent parity flips. An additional voltage contribution thus appears, which smears the voltage as a function of current near I_{c2} —just as in the region near I_{c1} discussed earlier.

Above I_{c2} none of the bands support minima, and the phase ϕ drifts continuously as in Fig. 3(d). The instantaneous drift velocity and hence also the voltage are nonetheless parity dependent. It follows that parity switching events, on average, produce a voltage $V \approx \mathcal{F}'_{\text{drift}} R \sqrt{I^2 - I_{c1}^2} + (1 - \mathcal{F}'_{\text{drift}}) R \sqrt{I^2 - I_{c2}^2}$. Here $\mathcal{F}'_{\text{drift}}$ and $1 - \mathcal{F}'_{\text{drift}}$ denote the fraction of time the phase spends in the potentials with critical currents I_{c1} and I_{c2} , respectively.

We thus arrive at the following overall picture for the high-bath-temperature case. When $\tau \gg \tau_R$ the *dc* voltage remains negligible as long as $I < I_{c1} = \min_{\mathbf{p}} I_{\mathbf{p},c}$. That is, contrary to the limit $T_b \ll \Delta$ the (lower) critical current as a function of flux follows the *minimum* of the critical currents associated with the four parity sectors. Furthermore, the critical current vanishes at zero flux and is maximal at one-half flux quantum—precisely as in a π -junction. These signatures are evident in the numerically computed in-

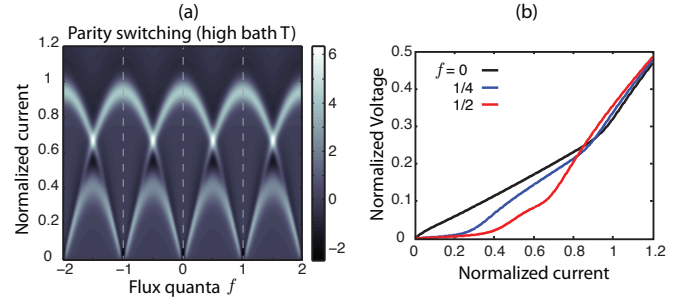


FIG. 4. (color online). (a) Color plot of d^2V/dI^2 and (b) voltage-current line cuts corresponding to the high-bath-temperature data in Fig. 2(d). The two critical currents I_{c1} and I_{c2} are clearly visible in both plots. Voltage and current are respectively expressed in units of $2eR\Delta/\hbar$ and $e\Delta/\hbar$.

terference pattern shown in Fig. 2(d). For $I > I_{c1}$ the voltage is far from featureless—a second critical current given by $I_{c2} = \max_{\mathbf{p}} I_{\mathbf{p},c}$ also appears, reflecting the multiple parity sectors that are sampled with roughly equal probability. This feature becomes prominent upon examining d^2V/dI^2 [Fig. 4(a)] as well as specific voltage-current line cuts [Fig. 4(b)]. Thus long parity-flip times τ allow one to image the critical currents in both the even *and* odd parity sectors. Rapid parity flipping with $\tau \ll \tau_R$, however, renders the junction resistive at any flux and yields identically zero critical current.

Discussion. Our study of extended QSH Josephson junctions reveals that parity switching processes, although destructive to the critical current’s anomalous periodicity, generate new fingerprints of the underlying topological superconductors expected to form. Surprisingly, stronger poisoning actually *enhances* the signatures in the critical current (as long as parity fluctuates on sufficiently long time scales). Absent knowledge of the system’s microscopic dynamics, we modeled parity switching using a bath that allows particles to hop into the unconventional Andreev bound states that mediate fractional Josephson currents at the junction ends. This model captures both the thermal and random parity-switching limits. We expect the results to apply quite generally—even when the actual switching mechanism differs. For instance, if the bound-state energies approach the continuum states near Δ then bulk quasiparticles can easily mediate parity flips [36]. Here we anticipate qualitatively similar behavior to the high-bath-temperature limit (which in a sense provides a ‘worst-case scenario’). We verified this numerically by changing the parity transition probabilities so that switching occurs predominantly at energies near Δ .

While our analysis has so far included only 4π -periodic current contributions, it is important to note that conventional 2π -periodic components $\propto \sin \delta\phi_{R/L}$ generically flow in parallel (though their magnitudes may be small). The Supplementary Material addresses the consequences of such terms. With low bath temperatures their effects are decidedly minor—the lifted nodes in Fig. 2(c) survive even for quite large conventional currents. More significant effects occur at high bath

temperature. There, the new terms lead to deviations from the π -junction behavior mimicked in Fig. 2(d). A finite critical current appears at zero flux (and all other integer flux quanta). Moreover, if the amplitude of the 2π -periodic current exceeds that of the 4π -periodic terms, the critical current becomes maximal at $f = 0$ and minimal at $f = 1/2$. The resulting interference pattern nevertheless *still* remains anomalous. Most importantly multiple critical currents remain visible in the current-voltage relation, which is the clearest indicator of topological superconductivity revealed by our study. The critical current, as with low bath temperatures, also remains finite for any magnetic field.

The absence of nodes in the critical current at half-integer flux quanta thus survives quite generally from the interplay between fractional Josephson physics and parity switching (Ref. [41] introduced a somewhat related mechanism). To provide a compelling indicator of topological superconductivity, however, the ability to experimentally distinguish from other node-lifting mechanisms such as current asymmetry is essential. This may be achieved by introducing a strong *in-plane* magnetic field, which can force the 1D topological superconductors at the junction into a trivial phase [7]. The phase transition eliminates the fractional Josephson physics, and with it the source of node-lifting that we have uncovered, while preserving the dominance of current flow at the junction edges. Observing the controlled destruction and revival of nodes as one varied the in-plane field strength would likely rule out alternative mechanisms and provide strong evidence for topological superconductivity.

Acknowledgements. We are indebted to D. Clarke, J. Meyer, J. Sau, A. Stern, D. van Harlingen, and especially B. Halperin, S. Hart, and H. Ren for enlightening discussions. We also acknowledge funding from the NSF through grants DMR-1341822 (S.-P. L. & J. A.) and DMR-1206016 (A. Y.); the Alfred P. Sloan Foundation (J. A.); a grant from Microsoft Corporation (A. Y.); and the Caltech Institute for Quantum Information and Matter, an NSF Physics Frontiers Center with support of the Gordon and Betty Moore Foundation. A. Y. is also supported by the STC Center for Integrated Quantum Materials, NSF grant DMR-1231319.

[1] A. Y. Kitaev, *Sov. Phys.-Uspeki* **44**, 131 (2001).
 [2] C. W. J. Beenakker, *Annu. Rev. Con. Mat. Phys.* **4**, 113 (2013).
 [3] J. Alicea, *Rep. Prog. Phys.* **75**, 076501 (2012).
 [4] M. Leijnse and K. Flensberg, *Semiconductor Science and Technology* **27**, 124003 (2012).
 [5] T. D. Stanescu and S. Tewari, *Journal of Physics: Condensed Matter* **25**, 233201 (2013).
 [6] C. Nayak, S. H. Simon, A. Stern, M. Freedman, and S. Das Sarma, *Rev. Mod. Phys.* **80**, 1083 (2008).
 [7] L. Fu and C. L. Kane, *Phys. Rev. B* **79**, 161408(R) (2009).
 [8] R. M. Lutchyn, J. D. Sau, and S. Das Sarma, *Phys. Rev. Lett.* **105**, 077001 (2010).
 [9] Y. Oreg, G. Refael, and F. von Oppen, *Phys. Rev. Lett.* **105**, 177002 (2010).

[10] A. Cook and M. Franz, *Phys. Rev. B* **84**, 201105 (2011).
 [11] T.-P. Choy, J. M. Edge, A. R. Akhmerov, and C. W. J. Beenakker, *Phys. Rev. B* **84**, 195442 (2011).
 [12] S. Nadj-Perge, I. K. Drozdov, B. A. Bernevig, and A. Yazdani, *Phys. Rev. B* **88**, 020407 (2013).
 [13] A. C. Potter and P. A. Lee, *Phys. Rev. B* **83**, 184520 (2011).
 [14] B. A. Bernevig, T. L. Hughes, and S.-C. Zhang, *Science* **314**, 1757 (2006).
 [15] M. König, S. Wiedmann, C. Brune, A. Roth, H. Buhmann, L. W. Molenkamp, X.-L. Qi, and S.-C. Zhang, *Science* **318**, 766 (2007).
 [16] A. Roth, C. Brune, H. Buhmann, L. W. Molenkamp, J. Maciejko, X.-L. Qi, and S.-C. Zhang, *Science* **325**, 294 (2009).
 [17] K. C. Nowack, E. M. Spanton, M. Baenninger, M. König, J. R. Kirtley, B. Kalisky, C. Ames, P. Leubner, C. Brüne, H. Buhmann, L. W. Molenkamp, D. Goldhaber-Gordon, and K. A. Moler, *Nature Materials* **12**, 787 (2013).
 [18] S. Hart, H. Ren, T. Wagner, P. Leubner, M. Mühlbauer, C. Brüne, H. Buhmann, L. W. Molenkamp, and A. Yacoby, *arXiv:1312.2559* (unpublished).
 [19] C. Liu, T. L. Hughes, X.-L. Qi, K. Wang, and S.-C. Zhang, *Phys. Rev. Lett.* **100**, 236601 (2008).
 [20] L. Du, I. Knez, G. Sullivan, and R.-R. Du, *arXiv:1306.1925* (unpublished).
 [21] E. M. Spanton, K. C. Nowack, L. Du, R.-R. Du, and K. A. Moler, *arXiv:1401.1531* (unpublished).
 [22] I. Knez, R.-R. Du, and G. Sullivan, *Phys. Rev. Lett.* **109**, 186603 (2012).
 [23] S. Mi, D. I. Pikulin, M. Wimmer, and C. W. J. Beenakker, *Phys. Rev. B* **87**, 241405 (2013).
 [24] C. W. J. Beenakker, J. M. Edge, J. P. Dahlhaus, D. I. Pikulin, S. Mi, and M. Wimmer, *Phys. Rev. Lett.* **111**, 037001 (2013).
 [25] F. Crepin, B. Trauzettel, and F. Dolcini, *arXiv:1401.0507* (unpublished).
 [26] A. M. Black-Schaffer and J. Linder, *Phys. Rev. B* **83**, 220511 (2011).
 [27] D. M. Badiane, M. Houzet, and J. S. Meyer, *Phys. Rev. Lett.* **107**, 177002 (2011).
 [28] L. Jiang, D. Pekker, J. Alicea, G. Refael, Y. Oreg, and F. von Oppen, *Phys. Rev. Lett.* **107**, 236401 (2011).
 [29] Q. Meng, V. Shivamoggi, T. L. Hughes, M. J. Gilbert, and S. Vishveshwara, *Phys. Rev. B* **86**, 165110 (2012).
 [30] L. Jiang, D. Pekker, J. Alicea, G. Refael, Y. Oreg, A. Brataas, and F. von Oppen, *Phys. Rev. B* **87**, 075438 (2013).
 [31] M. Houzet, J. S. Meyer, D. M. Badiane, and L. I. Glazman, *Phys. Rev. Lett.* **111**, 046401 (2013).
 [32] C. W. J. Beenakker, D. I. Pikulin, T. Hyart, H. Schomerus, and J. P. Dahlhaus, *Phys. Rev. Lett.* **110**, 017003 (2013).
 [33] S. Barbarino, R. Fazio, M. Sassetti, and F. Taddei, *New J. Phys.* **15**, 085025 (2013).
 [34] S.-F. Zhang, W. Zhu, and Q.-F. Sun, *Journal of Physics: Condensed Matter* **25**, 295301 (2013).
 [35] F. Crepin and B. Trauzettel, *arXiv:1305.7433* (unpublished).
 [36] D. M. Badiane, L. I. Glazman, M. Houzet, and J. S. Meyer, *arXiv:1310.5683* (unpublished).
 [37] V. Orlyanchik, M. P. Stehno, C. D. Nugroho, P. Ghaemi, M. Brahlek, N. Koirala, S. Oh, and D. J. Van Harlingen, *arXiv:1309.0163* (unpublished).
 [38] M. Tinkham, *Introduction to superconductivity, 2nd edition* (Dover, Mineola, New York, 1996).
 [39] V. Ambegaokar and B. I. Halperin, *Phys. Rev. Lett.* **22**, 1364 (1969).
 [40] H. Risken, *The Fokker-Planck equation* (Springer-Verlag, Berlin Heidelberg, 1989).

[41] A. C. Potter and L. Fu, Phys. Rev. B **88**, 121109 (2013).

SUPPLEMENTARY MATERIAL

1. Derivation of the generalized Fokker-Planck equation and the parity switching rate

The starting point for deriving the rate equation for the distribution function is the Master equation. The Master equation is based on the assumption that if one considers the density matrix, its non-diagonal elements can be neglected; only the diagonal ones corresponding to the distribution function are kept. In our case such a treatment is justified due to the macroscopic nature of the system. For the Josephson junctions discussed here, the distribution function depends on two variables: the phase ϕ and the parity vector \mathbf{p} . Assuming independent transitions in these variables, the Master equations reads

$$\begin{aligned} \partial_t \mathcal{P}_{\mathbf{p}}(\phi) = & \sum_{\phi'} [w_{\phi' \rightarrow \phi} \mathcal{P}_{\mathbf{p}}(\phi') - w_{\phi \rightarrow \phi'} \mathcal{P}_{\mathbf{p}}(\phi)] \\ & + \sum_{\mathbf{p}'} [W_{\mathbf{p}' \rightarrow \mathbf{p}} \mathcal{P}_{\mathbf{p}'}(\phi) - W_{\mathbf{p} \rightarrow \mathbf{p}'} \mathcal{P}_{\mathbf{p}}(\phi)]. \end{aligned} \quad (8)$$

Here, $w_{\phi \rightarrow \phi'}$ and $W_{\mathbf{p} \rightarrow \mathbf{p}'}$ are the transition rates between two different phase and parity states, respectively. For the continuous variable ϕ the over-damped RCSJ model yields

$$\begin{aligned} & \sum_{\phi'} [w_{\phi' \rightarrow \phi} \mathcal{P}_{\mathbf{p}}(\phi') - w_{\phi \rightarrow \phi'} \mathcal{P}_{\mathbf{p}}(\phi)] \\ & \rightarrow \frac{1}{\tau_R \Delta} \partial_\phi [\partial_\phi U_{\mathbf{p}}/2 + T \partial_\phi] \mathcal{P}_{\mathbf{p}}. \end{aligned} \quad (9)$$

Thus the first term in Eq. (8) is familiar from the conventional Fokker-Planck equation [39].

Next we will concentrate on the derivation of the parity transition rates. For this purpose we assume that the bound states connect to a particle source through a term in the Hamiltonian of the form $H_t = t \sum_{i=L,R} (d_i^\dagger f + f^\dagger d_i)$, where d_i (f) is the annihilation operator for an electron in bound state i (particle source). The index $i = L/R$ indicates the left and right bound state, so that the corresponding parity is $p_i = d_i^\dagger d_i$. The rate at which electrons transform from the particle bath to the bound state or vice versa can be approximated using Fermi's golden rule. For example, if $|p_L, p_R\rangle$ denotes the parity eigenstate for the junction then

$$\begin{aligned} W_{(0,p_R) \rightarrow (1,p_R)}(\phi) = & 2\pi t^2 |\langle 1, p_R | d_L^\dagger | 0, p_R \rangle|^2 \\ & \times \int d\omega g(\omega) n(\omega) \delta(U_{(1,p_R)} - U_{(0,p_R)} - \omega). \end{aligned} \quad (10)$$

The above equation describes absorption of an electron from the particle bath by the left bound state (a similar term can be written for the right bound state). Here $n(\omega)$ is the distribution function of the electron poisoning source and $g(\omega)$ is its density of states, with ω measured with respect to the chemical

potential. Possible sources of electrons that can hop into the bound states include—among others—subgap localized states and localized electrons in the bulk of the quantum spin Hall system. These different sources are uncorrelated and therefore can be modeled as an incoherent particle bath with a constant density of state, $g(\omega) \approx g_0$. The transition rate in Eq. (10) therefore becomes

$$W_{(0,p_R) \rightarrow (1,p_R)} = \frac{n[(U_{(1,p_R)} - U_{(0,p_R)})/T_b]}{\tau}. \quad (11)$$

with $1/\tau = 2\pi g_0 t^2$. Similarly, the transition rate for a particle hopping from the bound state into the bath reads:

$$\begin{aligned} W_{(1,p_R) \rightarrow (0,p_R)} = & 2\pi t^2 |\langle 0, p_R | d_L | 1, p_R \rangle|^2 \int d\omega g(\omega) \\ & \times [1 - n(\omega)] \delta(U_{(1,p_R)} - U_{(0,p_R)} - \omega) \\ = & \frac{n[(U_{(0,p_R)} - U_{(1,p_R)})/T_b]}{\tau}. \end{aligned} \quad (12)$$

Here we used the identity $1 - n(\omega) = n(-\omega)$. An equivalent treatment for the right bound state recovers the transition rates $W_{\mathbf{p} \rightarrow \mathbf{p}'}$ quoted in the main text.

Additional processes can contribute to the parity switching. For example, an electron can join a particle occupying the bound state and form a Cooper pair that hops into one of the superconducting leads. This process changes the parity from $(1, 0)$ to $(0, 0)$ by an absorption of a particle. The effect of such an event is to modify $1/\tau$ without changing the exponential term.

2. Influence of conventional supercurrent

The analysis performed in the main text assumed that the 4π -periodic fractional Josephson currents $I_{\mathbf{p}}(\phi, f)$ constituted the only supercurrent source in our extended QSH Josephson junction. We now analyze the more realistic case where ordinary Josephson currents—arising from continuum modes and/or additional Andreev bound states—flow in parallel. We will assume that these contributions, like the fractional Josephson currents, reside solely along the left and right junction ends in Fig. 1. Thus the total current for parity sector \mathbf{p} is taken to be

$$\tilde{I}_{\mathbf{p}}(\phi, f) = I_{\mathbf{p}}(\phi, f) + I_{2\pi}(\phi, f), \quad (13)$$

where

$$I_{2\pi}(\phi, f) = \frac{e\Delta_{2\pi}}{\hbar} [\sin \phi + \sin(\phi + 2\pi f)] \quad (14)$$

is the 2π -periodic component with an associated energy scale $\Delta_{2\pi}$. In terms of the energy $E_{2\pi}(\phi, f) = -\Delta_{2\pi} [\cos \phi + \cos(\phi + 2\pi f)]$ for states mediating the current in Eq. (14), the tilted washboard potentials that appear in the generalized Fokker-Planck equation are correspondingly modified to

$$\tilde{U}_{\mathbf{p}}(\phi, f) = E_{\mathbf{p}}(\phi, f) + E_{2\pi}(\phi, f) - \frac{\hbar I \phi}{e}. \quad (15)$$

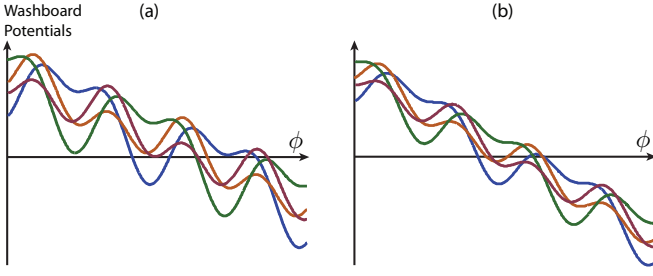


FIG. 5. (color online). Tilted washboard potentials including a 2π -periodic current component corresponding to $\Delta_{2\pi} = 0.8\Delta$ and $f = 1/4$. Parts (a) and (b) correspond to different applied currents. In (a) the current is sufficiently low that all potentials exhibit local minima roughly spaced by a phase difference of 2π due to the ordinary Josephson current. In (b) the blue and green potentials possess half as many local minima due to a higher applied current. Parity switching thus causes a slow drift of ϕ down the potentials so that a small dc voltage develops.

Note that the transition rates $W_{\mathbf{p} \rightarrow \mathbf{p}'}$ depend only on the unconventional bound-state energies $E_{\mathbf{p}}(\phi, f)$ since all other terms in the modified potentials are parity-independent.

Let us first revisit the low-bath-temperature limit $T_b \ll \Delta$. Here the parities again adjust such that the phase essentially follows the washboard potential $\tilde{U}(\phi, f) = \min_{\mathbf{p}} \tilde{U}_{\mathbf{p}}(\phi, f)$ that minimizes the total energy. In this regime non-zero $\Delta_{2\pi}$ renormalizes the ratio of the maximum and minimum critical currents in the interference pattern, but importantly preserves the lifted nodes that are indicative of topological superconductivity. At $f = (2n + 1)/2$ for integer n —where the node lifting arises—the conventional current indeed drops out entirely since $I_{2\pi}[\phi, f = (2n + 1)/2] = 0$.

The interplay between these two types of Josephson currents is more interesting at high bath temperature $T_b \gg \Delta$, where the system spends roughly equal time in all four parity sectors. Subsequent parity flips occur after a typical time scale τ which we will assume greatly exceeds τ_R . For concreteness we further assume that the energy scales for conventional and Josephson currents are comparable (other limits can be treated similarly). In this regime finite $I_{2\pi}$ leads to even richer structure in the current-voltage characteristics than in the $I_{2\pi} = 0$ case.

The additional structure can be anticipated upon examining the modified washboard potentials in Eq. (15). Consider the lowest current regime, where for a given \mathbf{p} the potential

$\tilde{U}_{\mathbf{p}}(\phi, f)$ features denser minima spaced by a phase difference of roughly 2π (instead of 4π as is the case with only fractional Josephson currents). As an example Fig. 5(a) displays the four washboard potentials at $f = 1/4$, $\Delta_{2\pi} = 0.8\Delta$, and low current. It is clear from the figure that parity flips no longer directly mediate $\pm 2\pi$ phase slips due to the additional minima; phase slips instead require thermal activation over a barrier.

At slightly larger currents the additional local minima generated by $I_{2\pi}$ disappear in some or all of the washboard potentials—see Fig. 5(b) which corresponds to the same parameters as (a) except for a higher current. Since all four washboard potentials still support local minima, the phase ϕ becomes trapped after each parity flip. Parity switching does, nevertheless, mediate a gradual drift down the potentials and hence produces a (small) dc voltage. For instance, beginning from a minimum of the red curve, a parity flip into the blue potential can cause the phase to wind rightward. Subsequent parity flips into the green curve will then cause a winding in the same direction. ‘Upstream’ drifting of the phase requires thermal activation and is thus suppressed compared to these processes. The magnitude of the dc voltage scales roughly as $V \sim \frac{eR\Delta}{\hbar} \frac{\tau_R}{\tau}$, where τ_R/τ captures the fraction of time during which the phase drifts.

As the current further increases a situation familiar from the main text arises: Half of the potentials lose *all* local minima leading to a much larger dc voltage since the phase drifts unimpeded in certain parity sectors. And finally in the highest current regime none of the potentials possess minima, and an even stronger voltage develops.

To summarize, incorporating a normal 2π -periodic current component into our generalized Fokker-Planck analysis not only preserves the multiple critical currents we identified previously at high bath temperature, but actually leads to additional current regimes and hence finer structure in the interference spectra. Figure 6 illustrates the voltage V and its second derivative d^2V/dI^2 as a function of I and f , along with specific voltage-current line cuts, for different conventional current strengths. The following points made in the main text are worth reiterating: (i) increasing $I_{2\pi}$ washes out the π -junction-like behavior in Fig. 2(d), (ii) with ‘large’ $I_{2\pi}$ the interference pattern resembles that at low bath temperature, and in particular features lifted nodes, and (iii) most importantly multiple critical currents remain visible even for substantial conventional currents.

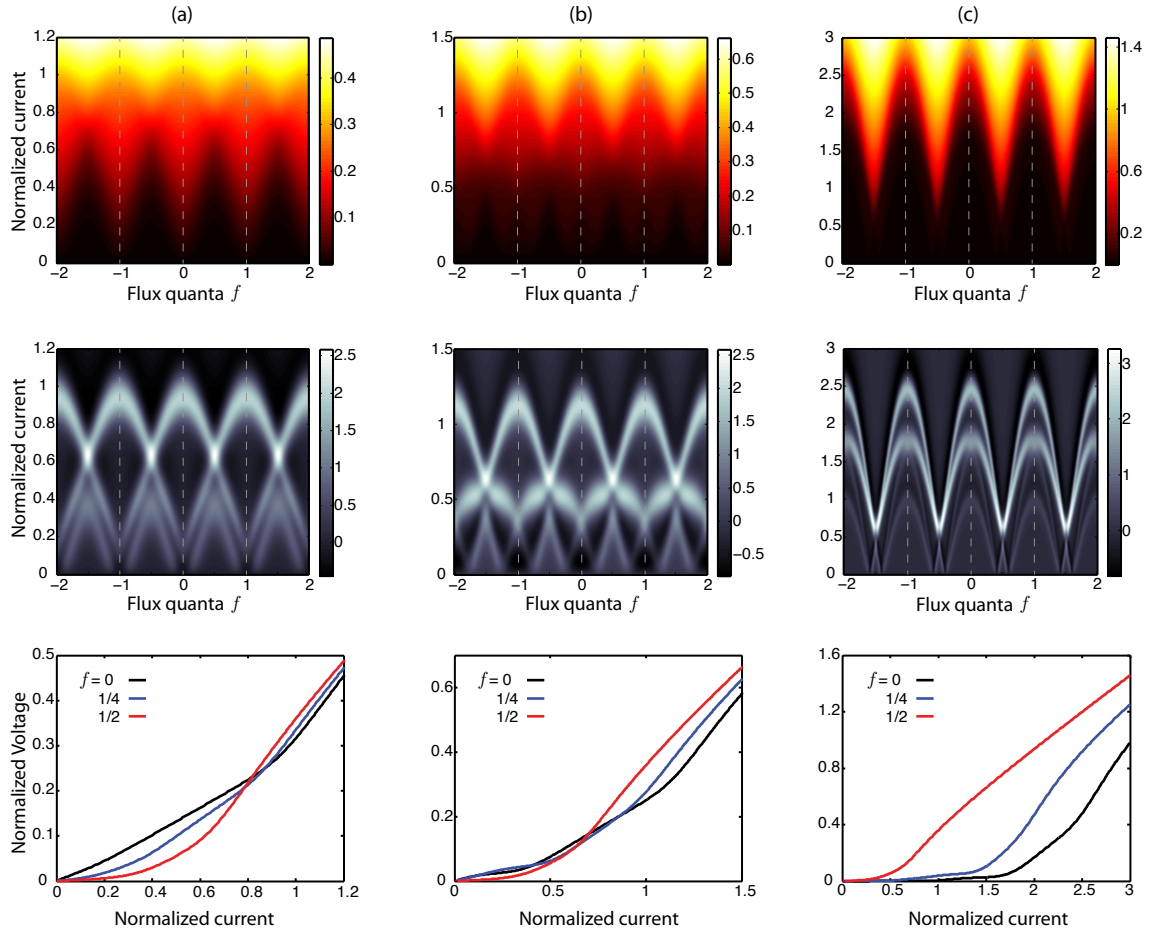


FIG. 6. (color online). Current-voltage characteristics reflecting the interplay between fractional and conventional Josephson currents at high bath temperature $T_b = 100\Delta$ and with a long parity relaxation time $\tau = 50\tau_R$. The color scale in the first and second rows indicates voltage V and its second derivative d^2V/dI^2 , respectively. The last row illustrates voltage-current line cuts at specific flux values. Going left to right the ordinary Josephson current increases, taking on values corresponding to (a) $\Delta_{2\pi} = 0.1\Delta$, (b) $\Delta_{2\pi} = 0.25\Delta$, and (c) $\Delta_{2\pi} = \Delta$. In all panels the junction temperature is $T = 0.05\Delta$, voltage is expressed in units of $2eR\Delta/\hbar$, and current is normalized by $e\Delta/\hbar$.